Inelastic electron scattering on C_{60} clusters

K. Yabana
Department of Physics, Niigata University, Niigata 950-21, Japan

G. F. Bertsch
Department of Physics and National Institute for Nuclear Theory, University of Washington, Seattle, Washington 98195

(Received 2 December 1993; accepted 4 January 1994)

We calculate the electronic excitation of C_{60} by inelastic electron scattering or electron energy loss spectroscopy (EELS). The scattering process is treated in the distorted-wave Born approximation, and the electronic excitations are calculated in a spherical basis model. We find that low energy electrons excite some nonphotoactive modes, in agreement with experiment. Spin triplet modes are poorly excited, even at the lowest electron energies.

I. INTRODUCTION

The spectroscopy of C_{60} is very simple for a large molecule, due to its high symmetry. For example, in photoabsorption measurements, only the excited states with T_{1u} symmetry are observed among the ten possible irreducible representations of icosahedral group I_h. This has been very helpful in establishing the structure of the molecule and in developing the theory of the electronic excitations. One would like to test the model Hamiltonians with other excitations besides those of T_{1u} symmetry, but the experimental information is more difficult to obtain and interpret.

Electron inelastic scattering provides one of the most useful ways to investigate electronic excitations in general. For low incident energy, there is no strict selection rule and all electronic excited states including the spin triplet states can be excited. The angular distribution of the scattered electrons will reflect the symmetry of the excited state.

High resolution electron inelastic scattering data are now available for C_{60} in the gas phase[1,2] and also in thin films,[3] using low-energy electrons to excite the molecule. Besides the peaks observed in the photoabsorption measurements, several new features are found in the 2–4 eV region. In this paper, we calculate electron inelastic scattering from C_{60}, concentrating on the region of the new features. There is also a feature at high energy loss that has been measured by EELS and interpreted using the plane wave Born approximation for the scattered electron.[4] However, low-energy electrons are strongly diffracted by the molecule and we shall therefore use the distorted-wave Born approximation (DWBA) for the scattering process. This approximation has been applied in the past to linear diatomic molecules.[5] We will also use a spherical basis to expand the wave functions of both the scattering and the bound electrons. This is motivated by the high symmetry of the C_{60} molecule, and it considerably simplifies the calculation.

The paper is organized as follows. We present the spherical-basis model for the electronic excitations in Sec. II. The wave function of the scattering electron is strongly distorted by the field of the molecule, and these distortion effects are discussed in Sec. III. The scattering is calculated with the full exchange interaction, according to formulas presented in Sec. IV. The results of the electronic excitations of C_{60} are presented and compared with experiment in Sec. V.

II. ELECTRONIC EXCITATIONS OF C_{60} IN A SPHERICAL BASIS MODEL

We have recently applied the spherical basis model to the electronic structure of C_{60}, calculating the single-particle orbitals and the dipole strength function.[6] In this section we shall use the model to describe the particle–hole excitation spectrum.

The electronic Hamiltonian for the 240 valence electrons is taken as

$$H=\sum_{i=1}^{240}\frac{p^2}{2m}+\sum_{i=1}^{240}\sum_{\alpha=1}^{60}\left[\frac{-Ze^2}{|\mathbf{r}_i-\mathbf{R}_\alpha|}+V_{\rm ps}(\mathbf{r}_i-\mathbf{R}_\alpha)\right]+\sum_{ij}^{240}\frac{e^2}{|\mathbf{r}_i-\mathbf{r}_j|}+\sum_{i}^{240}v_{\rm xc}[\rho(\mathbf{r}_i)]. \tag{2.1}$$

Here $\mathbf{r}_i(i=1,...,240)$ are the electron coordinates and $\mathbf{R}_\alpha(\alpha=1,...,60)$ represent the equilibrium positions of carbon ions. The ion charge number Z equals 4. The potential $V_{\rm ps}(\mathbf{r})$ represents the pseudopotential due to the core electrons. Finally, $v_{\rm xc}$ is an exchange-correlation potential[7] depending on the electron density $\rho(\mathbf{r}_i)$.

Including only the monopole part of the ion–electron Coulomb potential in Eq. (2.1), we obtain a spherical shell jellium Hamiltonian

$$H_{\rm jellium}=\sum_{i=1}^{240}\frac{p^2}{2m}-\sum_{i=1}^{240}60Z\frac{e^2}{r_{i>}}+\sum_{ij}^{240}\frac{e^2}{|\mathbf{r}_i-\mathbf{r}_j|}+\sum_{i}^{240}v_{\rm xc}[\rho(\mathbf{r}_i)], \tag{2.2}$$

where $r_{i>}$ represents larger between r_i and R, the radius of C_{60}. Applying the self-consistent local density approximation to the spherical shell jellium Hamiltonian of Eq. (2.2), we obtain a spherical self-consistent potential and a corresponding spherical density distribution. The self-consistent potential shows a deep valley at the radius of C_{60}. The single-

 0021-9606/94/100(8)/5580/8/$6.00

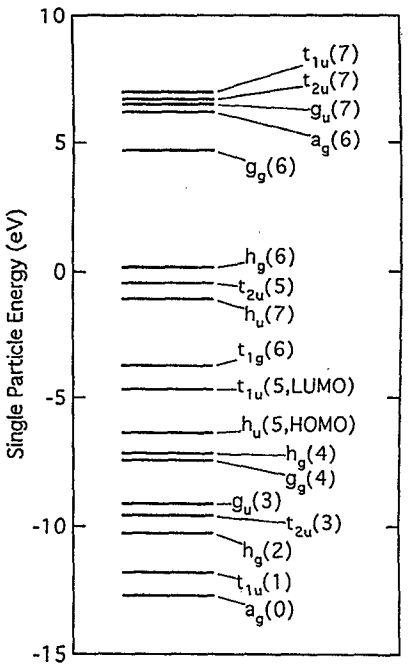

FIG. 1. Single particle spectrum in the spherical basis model for π-electron orbitals. The dominant angular momentum for each state is indicated in the parenthesis.

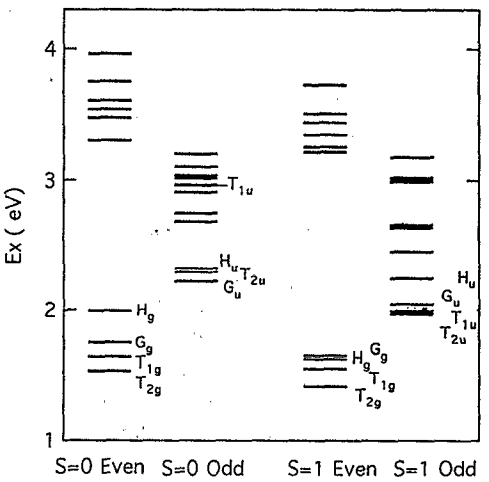

FIG. 2. Particle-hole spectrum in the spherical basis model. All the particle-hole states of the π-electron orbitals are included. The electron–electron interaction is weakened by factor 2, to take into account the σ-electron screening.

particle orbitals can be labeled by angular momentum and radial quantum numbers n. The states without radial nodes, namely, $n=0$, correspond to σ-electron orbitals, while the $n=1$ states correspond to π-electron orbitals. Both $n=0$ and $n=1$ orbitals are strongly localized near the radius R.

We mixed the states of different angular momentum with the nonspherical electron–ion potential but neglect its effect on the radial wave functions. The eigenstates no longer have the $(2l+1)$-fold degeneracy of the angular momentum states l but rather the degeneracies of the icosahedral group. Our calculation was not self-consistent in that we did not calculate the effect of the icosahedral symmetry-breaking on the electron contribution to the potential. Instead, we parametized the strength of the symmetry-breaking interaction, and found it possible to reproduce quite accurately in a spherical basis model the single-particle spectrum obtained with the fully self-consistent local density approximation.[6]

The single-particle wave function has the following structure:

$$\psi_n^{\Gamma i}(\mathbf{r})=\frac{u_n(r)}{r}\sum_{lm} C_{lm}^{\Gamma i}Y_{lm}(\hat{r}), \tag{2.3}$$

where the radial wave function is denoted by $u_n(r)$, and C_{lm}^{Γ} are coefficients of the different angular momentum eigenstates (l,m). The Γ labels the irreducible representation of the icosahedral group, and i distinguishes the degenerate electronic states belonging to the same Γ. The π–π^* transitions, that is, transitions among the states with $n=1$, dominate in the low-energy excitation spectrum, and we restrict our attention to these transitions in the following. In Fig. 1 we show the single-particle spectrum of the π electrons in the spherical basis model. The orbitals are bound or are sharp resonances for angular momenta up to $l=7$; only these orbitals are included in the diagonalization of the nonspherical interaction. The $l=5$ orbitals are split into three multiplets by the nonspherical interaction. The lowest of these, having h_u symmetry, is the highest occupied molecular orbital (HOMO). The next higher multiplet derived from the $l=5$ set of orbitals is the t_{1u} lowest unoccupied molecular orbital (LUMO). The energies of these states agree well with those calculated using more sophisticated approximations.[8]

With the single-particle orbitals described above, we construct the particle–hole states taking the hole from the 30 occupied spatial π orbitals and the particle from the unoccupied 34 spatial π orbitals. This yields 510 states of each parity, which are mixed by the residual electron–electron interaction. The residual electron–electron interaction should include the screening effects due to the σ electrons, since their polarization is not explicitly in the wave function of the configuration interaction calculation. We simply assume here that the residual interaction is the Coulomb interaction screened by factor 2 for all multipolarities. The spectrum obtained by diagonalizing the Hamiltonian matrix is shown in Fig. 2.

Previously the spectrum of particle–hole excitations has been computed in bases utilizing atomic orbitals.[9–11] Our calculations agree with these both in the ordering of multiplets within the major groups as well as the larger scale features of the spectrum, except when the multiplets are nearly degenerate. The excitation energy of the lowest triplet state is inferred from various experiments to lie at 1.6 eV, close to our calculated energy of 1.4 eV. Our odd-parity levels fit less well, lying about 0.8 eV lower than experiment. The lowest singlet T_{1u} state which is observed strongly in photoabsorption experiments has an energy of 3.8 eV, compared to our lowest T_{1u} at 3.0 eV. The lowest singlet T_{2u} state was assigned in our previous paper[11] to a state at 3.0 eV rendered

visible by vibronic coupling. Its energy is also shifted down in our calculation by about 0.8 eV. However, the difference between the lowest $^1T_{1u}$ and the lowest $^1T_{2u}$ states, which directly reflects the strength of the residual electron–electron interaction, is reasonable.

III. DISTORTING POTENTIAL FOR C_{60}

We now turn to the description of electron scattering from C_{60}. For low-energy incident electrons, say $E \leq 10$ eV, it is essential to include the distortion of the incoming and outgoing electron waves for a quantitative analysis of the angular distributions and cross sections. We deal with this by solving the Schrödinger equation for the electrons in the potential of the C_{60}.

We simplify here by considering only the spherically symmetric component of the electron potential. Because of the icosahedral symmetry of C_{60}, the potential will have components of multipolarities $L=6,10,12,\ldots$ as well. To argue for the neglect of these, we note that the $L=6$ component has only a small effect on the π orbital. The next multipole, $L=10$, has little effect on low partial waves up to $l=4$. However, as mentioned in the previous section, the HOMO-LUMO orbitals of π electrons are derived from $n=1$, $l=5$ orbitals in the spherical description. We should keep in mind that there might appear several resonances with $l=6,7$ character just above the threshold, which might strongly affect the scattering. These resonances will be split by the strong nonspherical interaction, and their detailed positions are not easy to predict.

As mentioned in Sec. I the scattering potential should be consistent with the bound state potential. We use the potential in Eq. (2.2) with three modifications. First, the scattered electron interacts with 240 bound electrons while bound electrons themselves are calculated with the field of the other 239 electrons only. The second difference is that the exchange-correlation interaction is modified due to the higher momentum of the scattering electron. We drop the local correlation contribution and take the exchange potential to have the form

$$V_{\rm exch}(r)=-\frac{e^2}{\pi}\,k_F(r)\left[1-\frac{k^2(r)-k_F^2(r)}{2k(r)k_F(r)}\times\log\frac{k(r)+k_F(r)}{k(r)-k_F(r)}\right], \tag{3.1}$$

where $k_F(r)$ is the local Fermi momentum, defined as usual by $k_F(r)=[3\pi^2\rho(r)]^{1/3}$. The local momentum of the scattered electron, $k(r)$, is determined by

$$\frac{\hbar^2k(r)^2}{2m}=E_{\rm in}+\frac{\hbar^2k_F(r)^2}{2m}+I \tag{3.2}$$

where $I=2.7$ eV is the electron affinity of C_{60},[12] and $E_{\rm in}$ is the incident electron's energy.

There is also long-range contribution to the potential from the polarization of the C_{60} by the scattering electron, which is not accounted for in the local density approximation. This potential is rather weak and not significant for the spectroscopy, but it can still have an important effect on the scattering of low energy electrons. For electron energies below 20 eV, we may assume the same polarizability as for static fields. We also consider only the dipole polarizability. The contribution to the potential then has the form

$$V_{\rm pol}(r)=-e^2\frac{\alpha}{r^4}\quad (r>R)$$
$$-e^2\frac{\alpha}{R^6}\,r^2\quad (r<R), \tag{3.3}$$

with R the radius of C_{60}. We take the value $\alpha=96$ Å^3 for the static polarizability, inferred from the measurement of index of refraction of solid C_{60} by the Clausius–Mosotti relation.

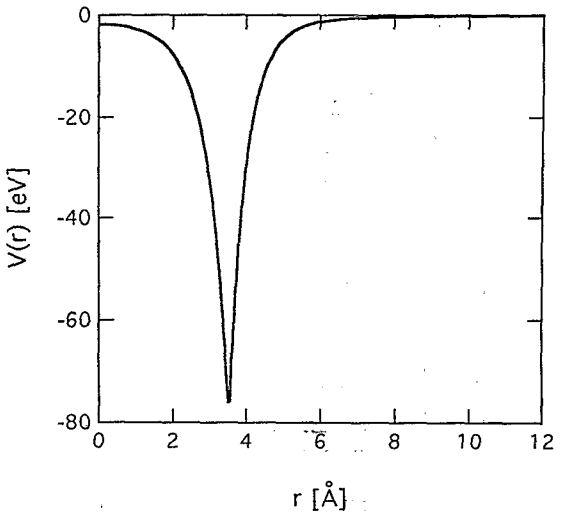

FIG. 3. Spherical distorting potential for the electron at $E_e=5$ eV.

We show in Fig. 3 the distorting potential at $E_{\rm inc}=5$ eV. The potential has a deep valley at the radius of C_{60}, and is close to the self-consistent spherical potential in the spherical shell jellium model discussed in the previous section. This potential produces a single-particle state with $n=1$, $l=5$ near the threshold. After including the icosahedral perturbation of nonspherical ion–electron interaction, the predicted LUMO of t_{1u} symmetry is at about -3 eV. Experimentally, the electron affinity of C_{60} is measured at 2.7 eV,[12] in good agreement with the present model.

For higher incident energy where the strongly coupled inelastic channels are open, an imaginary part of the distorting potential should also be included. However, without elastic data, it is difficult to make a reliable potential. In the present calculations we do not include the absorptive effect, which would tend to make our our predicted cross sections somewhat high.

IV. DISTORTED WAVE BORN APPROXIMATION

A. Formula for cross sections

In order to assess the relative importance of spin flip and higher multipolarities in the electron scattering, it is important to calculate the excitation with a full treatment of the exchange interaction between scattering and bound electrons.

We shall use the distorted wave Born approximation, whose basic formulas are given by the following equations (4.1)–(4.4). The differential cross section for the excitation of singlet states is given by

$$\left(\frac{d\sigma}{d\Omega}\right)_{i\to f}=\frac{v_f}{v_i}\left(\frac{m}{2\pi\hbar^2}\right)^2\frac{1}{2}\ |2T_{fi}^{\rm dir}-T_{fi}^{\rm exch}|^2 \tag{4.1}$$

and the cross section for triplet state excitation is

$$\left(\frac{d\sigma}{d\Omega}\right)_{i\to f}=\frac{v_f}{v_i}\left(\frac{m}{2\pi\hbar^2}\right)^2\frac{3}{2}\ |T_{fi}^{\rm exch}|^2. \tag{4.2}$$

In these two equations the direct and the exchange T matrices are defined as

$$T_{fi}^{\rm dir}=\int d\mathbf{r}\,d\mathbf{r}'\ \psi_{\mathbf{k}_f}^{(-)*}(\mathbf{r})\psi_{\mathbf{k}_i}^{(+)}(\mathbf{r})\frac{e^2}{|\mathbf{r}-\mathbf{r}'|}\ \rho_{fi}(\mathbf{r}'),$$

$$T_{fi}^{\rm exch}=\int d\mathbf{r}\,d\mathbf{r}'\ \psi_{\mathbf{k}_f}^{(-)*}(\mathbf{r})\psi_{\mathbf{k}_i}^{(+)}(\mathbf{r}')\frac{e^2}{|\mathbf{r}-\mathbf{r}'|}\ \rho_{fi}(\mathbf{r}',\mathbf{r}) \tag{4.3}$$

where

$$\rho_{fi}(\mathbf{r},\mathbf{r}')=\langle\Psi_f|a_{\mathbf{r}}^\dagger a_{\mathbf{r}'}|\Psi_i\rangle \tag{4.4}$$

is the transition density matrix and $\rho_{fi}(\mathbf{r})\equiv\rho_{fi}(\mathbf{r},\mathbf{r})$ is the ordinary transition density.

In our model, the transition density for π–π^* transitions has the following form:

$$\rho_\alpha(\mathbf{r},\mathbf{r}')=\frac{u(r)}{r}\frac{u(r')}{r'}\times\sum_{l_pm_pl_hm_h}A^{(\alpha)}_{l_pm_pl_hm_h}Y^*_{l_pm_p}(\hat{r})Y_{l_hm_h}(\hat{r}'), \tag{4.5}$$

where $u(r)\equiv u_1(r)$ is the radial wave function of the π orbital. $(n=1)$. The coefficients $A^{(\alpha)}_{l_pm_pl_hm_h}$ are the particle–hole amplitudes of the eigenstate α in the configuration interaction calculation discussed in Sec. II. Our model does not include screening effects of the σ or π electrons. This will make the predicted cross sections too large. We thus can only use our model to assess relative cross sections.

To numerically evaluate the scattering wave functions we make a multipole expansion as

$$\psi_{\mathbf{k}}^{(+)}(\mathbf{r})=\sum_l 4\pi i^l e^{i\delta_l}\frac{F_l(k,r)}{r}\sum_m Y^*_{lm}(\hat{k})Y_{lm}(\hat{r}). \tag{4.6}$$

The radial wave function $F_l(k,r)$ is obtained by numerically solving the radial Schrödinger equation. The T matrix is now expressed in the following way:

$$T_{fi}^{\rm dir,exch}=e^2(4\pi)^3\sum_{l_fm_fl_im_i}i^{l_i-l_f}e^{i(\delta_{l_i}+\delta^*_{l_f})}Y_{l_fm_f}(\hat{k}_f)\times Y^*_{l_im_i}(\hat{k}_i)X^{\rm dir,exch}_{fi,l_fm_fl_im_i} \tag{4.7}$$

in terms of the partial waves l_i and l_f of the incoming and outgoing scattered electron. The coefficient $X^{\rm dir}$ is given by

$$X^{\rm dir}_{fi,l_fm_fl_im_i}=\sum_{LML_pM_pL_hM_h}\frac{1}{2L+1}\ t^{\rm dir}_{l_fl_iL}\langle l_fm_f|Y_{LM}|l_im_i\rangle\times\langle L_hM_h|Y_{LM}|L_pM_p\rangle A^{(fi)}_{L_pM_pL_hM_h}, \tag{4.8}$$

where $t^{\rm dir}$ is the radial integral

$$t^{\rm dir}_{l_fl_iL}=\int_0^\infty dr\ dr'\ F^*_{l_f}(k_f,r)F_{l_i}(k_i,r)\{u(r')\}^2\frac{r_<^L}{r_>^{L+1}}. \tag{4.9}$$

Similarly, $X^{\rm exch}$ is given by

$$X^{\rm exch}_{fi,l_fm_fl_im_i}=\sum_{LML_pM_pL_hM_h}\frac{1}{2L+1}\ t^{\rm exch}_{l_fl_iL}\langle l_fm_f|Y_{LM}|L_hM_h\rangle\times\langle l_im_i|Y_{LM}|L_pM_p\rangle A^{(fi)}_{L_pM_pL_hM_h} \tag{4.10}$$

with the exchange radial integral

$$t^{\rm exch}_{l_fl_iL}=\int_0^\infty dr\ dr'\ F^*_{l_f}(k_f,r)F_{l_i}(k_i,r')u(r)u(r')\frac{r_<^L}{r_>^{L+1}}. \tag{4.11}$$

The above formulas determine the differential cross section for fixed positions of the ions. Since we do not resolve the molecular rotation spectra, we should add the cross sections including rotational excitation. Assuming the rotational energies much smaller than the electronic excitation energy, the summation over rotational excitations are equivalent to averaging the cross section over possible orientations of the molecule.

The calculation of Eq. (4.7) is already numerically time consuming, and a further sum over orientations would be beyond our resources. Fortunately, this is not necessary if we average over directions of the incident electron instead. To make this average, we note that the absolute square of the T matrices has the following dependence on the directions of the incident and outgoing electrons:

$$|T_{fi}(\mathbf{k}_f,\mathbf{k}_i)|^2=\sum_{L_fM_fL_iM_i}G_{L_fM_fL_iM_i}(k_f,k_i)\times Y_{L_fM_f}(\hat{k}_f)Y^*_{L_iM_i}(\hat{k}_i). \tag{4.12}$$

The average of Eq. (4.12) is made using the fact

$$\int\frac{d\Omega}{8\pi^2}\ [Y_{L_fM_f}(\hat{R}_\Omega(\hat{k}_f))Y^*_{L_iM_i}(\hat{R}_\Omega(\hat{k}_i))]=\frac{1}{4\pi}\ \delta_{L_fL_i}\delta_{M_fM_i}P_{L_i}(\cos\Theta), \tag{4.13}$$

where $P_L(x)$ is the Legendre polynomial and Θ represents the relative angle between $\hat{k}_f$ and $\hat{k}_i$, that is, the scattering angle. The R_Ω represents the rotation operator for the Euler angles Ω.

Finally, the differential cross section after averaging over orientations is given by

$$\left\langle \left(\frac{d\sigma}{d\Omega}\right)_{fi} \right\rangle_{\rm av} = \frac{v_f}{v_i}\left(\frac{m}{2\pi\hbar^2}\right)^2 e^4(4\pi)^5 \sum_{l_f m_f l_i m_i l_f' m_f' l_i' m_i' LM} i^{l_i - l_f - l_i' + l_f'} e^{i(\delta_{l_i}^* + \delta_{l_f} - \delta_{l_i'}^* - \delta_{l_f'})} \frac{1}{2}\,(2X^{\rm dir}_{l_f m_f l_i m_i} - X^{\rm exch}_{l_f m_f l_i m_i})$$
$$\times (2X^{\rm dir*}_{l_f' m_f l_i' m_i'} - X^{\rm exch*}_{l_f' m_f' l_i' m_i'}) P_L(\cos\Theta)\langle l_f m_f | Y_{LM} | l_f' m_f'\rangle \langle l_i m_i | Y_{LM} | l_i' m_i'\rangle, \tag{4.14}$$

and a similar expression is obtained for the triplet excitation. The expression for the angle integrated cross section is much simpler, requiring only a fourfold sum over angular momentum indices,

$$\sigma_{fi} = \frac{v_f}{v_i}\left(\frac{m}{2\pi\hbar^2}\right)^2 e^4(4\pi)^5 \times \sum_{l_f m_f l_i m_i} \frac{1}{2}\,|2X^{\rm dir}_{l_f m_f l_i m_i} - X^{\rm exch}_{l_f m_f l_i m_i}|^2. \tag{4.15}$$

Again, a similar formula is found for the angle-integrated triplet excitation cross section.

B. Plane wave limit

Although the distortion will be strong for C_{60}, the plane wave limit is useful to understand the qualitative behavior. It will also be useful numerically for the very forward angles where the distortion effect is small and where the convergence of the sum over partial waves is poor.

We only discuss the direct term which is dominant at forward angles. The T matrix is given in the plane-wave Born approximation by

$$T_{fi}^{\rm dir}(\mathbf{q}) = \frac{4\pi e^2}{q^2}\int d\mathbf{r}\, e^{-i\mathbf{q}\mathbf{r}}\rho_{fi}(\mathbf{r}), \tag{4.16}$$

where $\mathbf{q}=\mathbf{k}_f-\mathbf{k}_i$ is the momentum transfer. Using the explicit form of the transition density given by Eq. (4.5), the T matrix may be expressed

$$T_{fi}(\mathbf{q}) = \sum_{LM} 4\pi(-i)^L \tilde{\rho}_{fi,LM} Y_{LM}(\hat{q}) \int dr\; j_L(qr) u^2(r), \tag{4.17}$$

where the multipole moments of the transition density $\tilde{\rho}_{fi,LM}$ are defined by

$$\int d\hat{r}\; Y_{LM}^*(\hat{r})\rho_{fi}(\mathbf{r}) = \frac{u^2(r)}{r^2}\,\tilde{\rho}_{fi,LM}. \tag{4.18}$$

After averaging over orientations of the cluster, the differential cross section for the singlet excited state is found to be

$$\left\langle \left(\frac{d\sigma}{d\Omega}\right)_{fi} \right\rangle_{\rm av} = \frac{v_f}{v_i}\left(\frac{m}{2\pi\hbar^2}\right)^2 2\left(\frac{4\pi e^2}{q^2}\right)^2 4\pi \times \sum_L \left\{\int dr\; j_L(qr)u(r)^2\right\}^2 \sum_M |\tilde{\rho}_{fi,LM}|^2. \tag{4.19}$$

Since $u(r)$ is peaked at the radius of C_{60}, the radial integral is approximately given by $j_L(qR)$. For low momentum transfer, only multipolarities with small L are important. The strong transitions will then be to states which contain low L. This depends on the representation Γ of the icosahedral group; the lowest L of different representations are given in Table I. The strongest states at forward angles should be states with T_{1u} and H_g symmetry, since they can carry $L=1$ and 2. There are no low electronic excitations of A_g symmetry, which would also be strong by this argument. This approximate selection rule will be useful to understand the distorted wave results and their comparison with measurements.

V. RESULTS AND DISCUSSION

EELS data at low bombarding energy[1–3] show some structures in the low excitation region which are absent in the photoabsorption measurements. These include peaks at 2.2 and at 3.0 eV, below the dipole excitations starting at 3.8 eV. There is also a weak feature observed at 1.5 eV in the thin film data.

We will attempt an assignment of the electronic excitations for the observed peaks, making use of the DWBA calculations. The gas phase data has the energy of outgoing electrons fixed at 3 eV, and we will calculate the DWBA cross sections under these conditions. We set the excitation energy of the low lying states to the average value, 2 eV for the even parity and 3.5 eV for the odd parity excitations. The incident electron energies are then 5 eV for even parity and 6.5 eV for odd parity excitations. We include the partial waves of the incoming and outgoing waves up to $l=12$, much larger than the classical grazing angular momentum $k_iR\sim 4.6$. However, as will be seen, this cutoff on l is not sufficient for convergence of the low multipole excitation cross sections at forward angles.

In Table II(a), we show the integrated cross sections for the low lying excitations. The states are the lowest of each symmetry, and are marked in the excitation spectrum of Fig. 2. From the table it may be seen that the integrated cross sections exciting singlet states depend strongly on the par-

TABLE I. Lowest multipolarity L in the representations Γ of the icosahedral group.

Γ	L
A_g	0
T_{1u}	1
H_g	2
T_{2u}	3
G_u	3
G_g	4
H_u	5
T_{1g}	6
T_{2g}	8
A_u	

TABLE II. The integrated cross sections (a) and the forward angle differential cross sections (b) for the electron inelastic scatterings to low lying electronic excitations. Final electron energy is set to 3 eV.

(a) Integrated cross sections (Å^2)

$S=0$				$S=1$			
Even		Odd		Even		Odd	
T_{2g}	0.485	G_u	0.605	T_{2g}	3.179	T_{2u}	2.457
T_{1g}	0.519	T_{2u}	1.434	T_{1g}	2.151	T_{1u}	2.778
G_g	1.105	H_u	0.709	H_g	3.617	G_u	2.763
H_g	19.748	T_{1u}	15.237	G_g	2.318	H_u	2.319

(b) Forward angle differential cross sections (Å^2/Sr)

$S=0$				$S=1$			
Even		Odd		Even		Odd	
T_{2g}	0.009	G_u	0.074	T_{2g}	0.085	T_{2u}	0.937
T_{1g}	0.003	T_{2u}	0.332	T_{1g}	0.043	T_{1u}	2.692
G_g	0.055	H_u	0.039	H_g	0.319	G_u	0.338
H_g	8.414	T_{1u}	41.358	G_g	0.121	H_u	0.213

ticular state involved, but the cross sections are nearly the same for different triplet excitations. This follows from the character of the interaction. For triplet excitations, only the exchange interaction contributes. It requires high momentum transfer and so does not exhibit particular selectivity with respect to the spatial symmetry of the excitation. The singlet excitations are dominated by the direct interaction for low momentum transfer, and this produces very large cross sections for low multipolarities. As we discussed in Sec. IV B the cross section for the direct process depends on the momentum transfer as $q^{-4}[j_L(qR)]^2$ with R the radius of C_{60}, in the plane wave limit. It appears that the direct process dominates for singlet excitations of states containing $L \leqslant 3$, and the exchange process is as important for other states.

The cross sections for exchange scattering are much smaller than the low-L singlet excitation cross sections, even at the lowest incident energy. There does not seem to be any preference among states of different icosahedral symmetry, reflecting the large momentum transfer. All the triplet excitations are excited nearly equally, though the forward cross sections show some selectivity for the low multipole excitations.

A. Assignment for the observed peaks

It seems likely that the $^1T_{1u}$ state should be assigned to the observed photoabsorption peak at 3.8 eV. The only other low state that has a substantial cross section in our model is the ^1H_g state. The predicted excitation energy of this state is about 2 eV in our model and 2.5 eV in Ref. 9. Thus we feel confident that the observed peak at 2.2 eV should be assigned to the H_g configuration. (Note however that Ref. 10 predicts the lowest ^1H_g at 3.15 eV.) Quantitatively, the experiment shows stronger excitation of the 2.2 eV peak than the dipole-allowed peak at 3.8 eV.[1]

Table II(b) displays the differential cross sections in the forward direction. Although our calculation predicts a larger integrated cross section for the ^1H_g than the $^1T_{1u}$ state, the H_g is weaker in the forward direction. Two deficiencies of our calculation may be responsible. First, as will be discussed, the partial wave expansion is not fully converged in our calculation for forward scattering. Second, the long-range Coulomb interaction should be screened by the polarization of the C_{60}. Screening would be stronger for the lower multipole state and reduce more efficiently the $^1T_{1u}$ excitation than ^1H_g excitation.

We cannot assign definitely the structure at 3 eV, but there are several possibilities. In view of the energy spectrum of Fig. 2, the excitation is probably one of the odd parity states. The integrated cross sections are nearly the same exciting the $^1T_{2u}$ state or one of the triplet states. At the forward angles relevant to the EELS measurments, the $^3T_{1u}$ state has the largest differential cross section, and so this assignment would be preferred.

On the other hand, in the optical absorption measurement, two clear peaks are observed around 3.1 eV.[13] We previously made an analysis in which we concluded that these states are vibrational modes built on the $^1T_{2u}$ electronic excitation.[11] Therefore, it is also quite plausible to assign the peak at 3.0 eV as the $^1T_{2u}$. The fact that the peak at 3 eV is very sharp from the EELS data on the gas phase,[1] in contrast to the broad features of 2.2 and 3.8 eV, is also consistent with this interpretation, since the optical absorption peaks at 3.1 eV are also quite sharp.[9] At this point, it is difficult to make a definite assignment selecting between the two possibilities, the $^1T_{2u}$ and the $^3T_{1u}$ excitations.

B. Angular distribution

Though the measurements of the angular distributions of the scattered electrons are not available yet, they reflect the excitation structures and are useful for the spectroscopic studies. We present some calculations of the angular distribution.

In Fig. 4, we show angular distributions of the three singlet excitations, $^1T_{1u}$, ^1H_g, and $^1T_{2u}$. They are characterized by their lowest allowed multipoles, which are $L=1,2,3$, respectively. The differential cross sections are forward

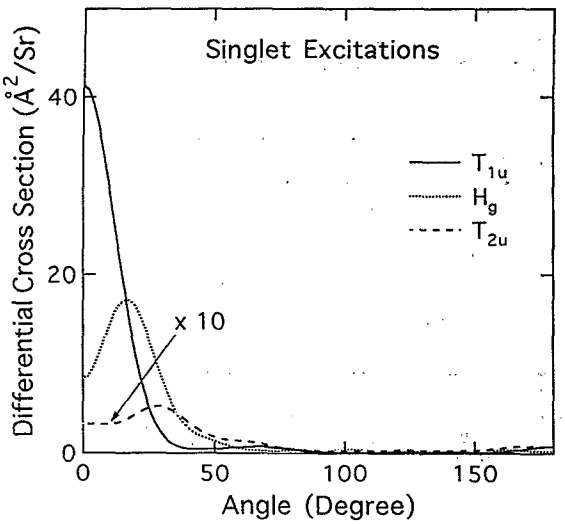

FIG. 4. Angular distribution for the singlet excitations ${}^1T_{1u}$, ${}^1H_g$, and ${}^1T_{2u}$, calculated by the DWBA. The outgoing electron energy is set to 3 eV.

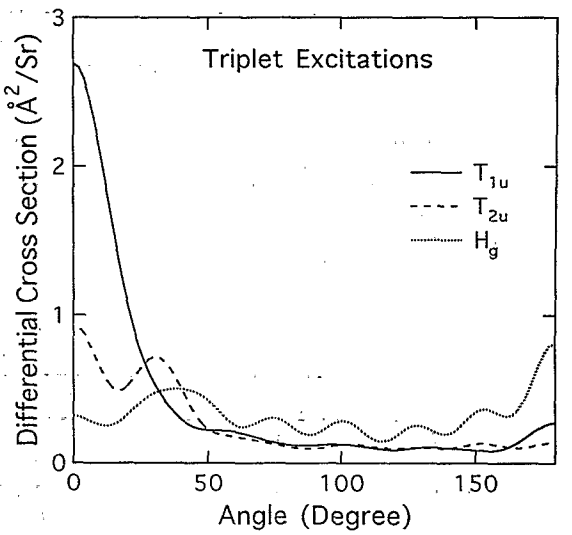

FIG. 6. Angular distribution for the triplet excitations ${}^3T_{1u}$, ${}^3T_{2u}$, and ${}^3H_g$, calculated by the DWBA. The outgoing electron energy is set to 3 eV.

peaked, with the smaller angular range for the lower multipole excitations.

Figure 5 shows the comparison of the distorted wave Born and the plane wave Born approximations for the ${}^1H_g$ excitations. The plane wave Born results are calculated with two ways: the formula of Sec. IV B which include all the partial waves of the incoming and outgoing waves, and the DWBA code without the distorting potential. The comparison of the two plane wave calculations thus shows the convergence of the calculation with respect to the partial wave expansion up to $l=12$.

At very forward angles, the plane wave calculation with partial wave cutoff underestimates the cross section by 30%. The DWBA calculation may underestimate the same amount of the cross section at forward direction. Though the angular distributions show difference, the integrated cross sections coincide to an accuracy within 1%. The difference between two plane wave calculations is largest for the ${}^1H_g$ state in the present calculation.

Compared with the plane wave result, the DWBA cross section is reduced significantly, showing the importance of the distortion effect for the quantitative analysis.

In Fig. 6, the angular distributions for some triplet excitations are shown. The angular distribution is flat for many excitations, reflecting various multipole contribution to average the cross section. The ${}^3T_{1u}$ excitation is exceptional, showing a forward peaked angular distribution. The ${}^3T_{2u}$ excitation included in the figure is the lowest electronic excitation, which may be responsible for the 1.5 eV structure observed in the thin film data.[3]

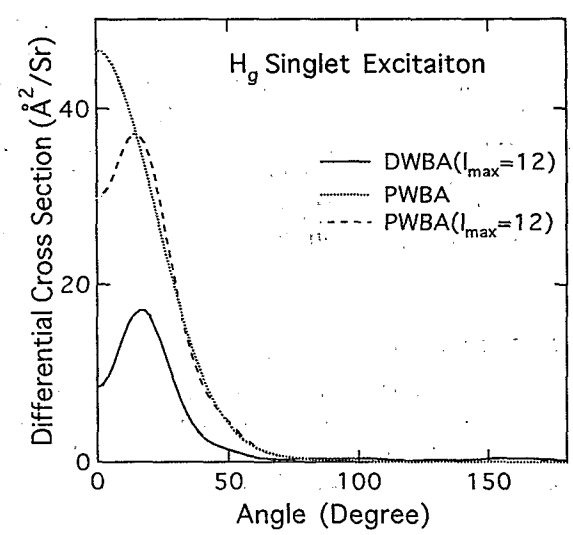

FIG. 5. Angular distribution for the ${}^1H_g$ excitation, comparing the DWBA and the PWBA. In the PWBA calculation, the calculations are shown with and without the partial wave expansion of the scattered electron.

VI. SUMMARY

We developed a theoretical framework for interpreting EELS measurements on C_{60}. We rely on a spherical basis for constructing wave functions both for the electronic excitations and the scattering electrons.

Besides the dipole allowed excitations, a singlet excitation with H_g symmetry, which includes $L^{\pi}=2^+$ component, is found to be excited strongly, and is assigned to the observed structure around 2.2 eV in the EELS measurement.

The singlet excitations in the low incident energy follow the formula in the long wavelength limit of the plane wave approximation, where the cross section for the excitation of multipole L is proportional to $q^{-4}[j_L(qR)]^2$ with R the radius of C_{60}. The triplet excitations are weak and do not show the selectivity of the final excitations, reflecting the large momentum transfer associated with the exchange process.

ACKNOWLEDGMENTS

One of the authors (K.Y.) is grateful for the hospitality of INT, Univ. of Washington, where this work was initiated. Financial support was provided by the Department of Energy under Grant No. DE-FG06-90ER40561.

[1] C. Bulliard, M. Allan, and S. Leach, Chem. Phys. Lett. **209**, 434 (1993).
[2] A. Burose, T. Dresch, and A. Ding, Z. Phys. D **26**, (1993), S294.
[3] A. Lucas, G. Gensterblum, J. J. Pireaux, P. A. Thiry, R. Caudano, J. P. Vigneron, Ph. Lambin, and W. Krätschmer, Phys. Rev. B **45**, 13694 (1992).
[4] A. Bulgac and N. Ju, Phys. Rev. B **46**, 4297 (1992).
[5] A. Fliflet and V. McKoy, Phys. Rev. A **21**, 1863 (1980).
[6] K. Yabana and G. F. Bertsch, Phys. Scripta (in press).
[7] O. Gunnarsson and B. Lundqvist, Phys. Rev. B **13**, 4274 (1976).
[8] J. W. Mintmire, B. I. Dunlap, D. W. Brenner, R. C. Mowrey, and C. T. White, Phys. Rev. B **43**, 14281 (1991); B. I. Dunlap, D. W. Brenner, J. W. Mintmire, R. C. Mowrey, and C. T. White, J. Phys. Chem. **95**, 5763 (1991); S. Saito and A. Oshiyama, Phys. Rev. Lett. **66**, 2637 (1991); J. L. Martins, N. Troullier, and J. H. Weaver, Chem. Phys. Lett. **180**, 457 (1991); J. H. Weaver, J. L. Martins, T. Komeda, Y. Chen, T. R. Ohno, G. H. Kroll, N. Troullier, R. E. Haufler, and R. E. Smalley, *ibid.* **66**, 1741 (1991); H. P. Lüthi and J. Almlöf, Chem. Phys. Lett. **135**, 357 (1987); P. W. Fowler, P. Lazzeretti, and R. Zanasi, *ibid.* **165**, 79 (1990); W. Y. Ching, M.-Z. Huang, Y.-N. Xu, W. G. Harter, and F. T. Chan, Phys. Rev. Lett. **67**, 2045 (1991); L. Ye, A. J. Freeman, and B. Delley, Chem. Phys. **160**, 415 (1992); V. de Coulon, J. L. Martins, and F. Reuse, Phys. Rev. B **45**, 13671 (1992).
[9] S. Larsson, A. Volosov, and A. Rosen, Chem. Phys. Lett. **133**, 501 (1987).
[10] F. Negri, G. Orlandi, and F. Zerbetto, Chem. Phys. Lett. **144**, 31 (1988).
[11] K. Yabana and G. F. Bertsch, Chem. Phys. Lett. **197**, 32 (1992).
[12] S. H. Yang, C. L. Pettiette, J. Conceicao, O. Cheshnovsky, and R. E. Smalley, Chem. Phys. Lett. **139**, 233 (1987).
[13] R. L. Whetten, M. M. Alvarez, S. J. Anz, K. E. Schriver, R. D. Beck, F. N. Diederich, Y. Rubin, R. Ettl, C. S. Foote, A. P. Darmanyan, and J. W. Arbogast, Mat. Res. Soc. Symp. Proc. **206**, 639 (1991); Z. Gasyna, P. N. Schatz, J. P. Hare, T. J. Dennis, H. W. Kroto, P. Taylor, and D. R. M. Walton, Chem. Phys. Lett. **183**, 283 (1991); R. E. Haufler, Y. Chai, L. P. F. Chibante, M. R. Fraelich, R. B. Weisman, R. F. Curl, and R. E. Smalley, J. Chem. Phys. **95**, 2197 (1991).